Biochemical and Biophysical Research Communications 403 (2010) 214–219

Contents lists available at ScienceDirect

Biochemical and Biophysical Research Communications

journal homepage: www.elsevier.com/locate/ybbrc

Thermal-induced conformational changes in the product release area drive the enzymatic activity of xylanases 10B: Crystal structure, conformational stability and functional characterization of the xylanase 10B from *Thermotoga petrophila* RKU-1

Camila Ramos Santos [a], Andreia Navarro Meza [a], Zaira Bruna Hoffmam [b], Junio Cota Silva [b], Thabata Maria Alvarez [b], Roberto Ruller [b], Guilherme Menegon Giesel [c], Hugo Verli [c], Fabio Marcio Squina [b], Rolf Alexander Prade [d], Mario Tyago Murakami [a,*]

[a] *Laboratório Nacional de Biociências (LNBio), Centro Nacional de Pesquisa em Energia e Materiais, Campinas, SP, Brazil*
[b] *Laboratório Nacional de Ciência e Tecnologia do Bioetanol (CTBE), Centro Nacional de Pesquisa em Energia e Materiais, Campinas, SP, Brazil*
[c] *Centro de Biotecnologia, Universidade Federal do Rio Grande do Sul, Porto Alegre, RS, Brazil*
[d] *Department of Microbiology and Molecular Genetics, Oklahoma State University, Stillwater, OK, USA*

ARTICLE INFO

Article history:
Received 27 October 2010
Available online 9 November 2010

Keywords:
Xylanase
Glycoside hydrolase family 10
Crystal structure
Thermostability
Thermotoga petrophila RKU-1

ABSTRACT

Endo-xylanases play a key role in the depolymerization of xylan and recently, they have attracted much attention owing to their potential applications on biofuels and paper industries. In this work, we have investigated the molecular basis for the action mode of xylanases 10B at high temperatures using biochemical, biophysical and crystallographic methods. The crystal structure of xylanase 10B from hyperthermophilic bacterium *Thermotoga petrophila* RKU-1 (TpXyl10B) has been solved in the native state and in complex with xylobiose. The complex crystal structure showed a classical binding mode shared among other xylanases, which encompasses the −1 and −2 subsites. Interestingly, TpXyl10B displayed a temperature-dependent action mode producing xylobiose and xylotriose at 20 °C, and exclusively xylobiose at 90 °C as assessed by capillary zone electrophoresis. Moreover, circular dichroism spectroscopy suggested a coupling effect of temperature-induced structural changes with this particular enzymatic behavior. Molecular dynamics simulations supported the CD analysis suggesting that an open conformational state adopted by the catalytic loop (Trp297-Lys326) provokes significant modifications in the product release area (+1,+2 and +3 subsites), which drives the enzymatic activity to the specific release of xylobiose at high temperatures.

1. Introduction

Xylanases (β-1,4-xylan xylanohydrolase, E.C. 3.2.1.8) are responsible for breaking down xylan, the major hemicellulosic component of plant cell walls, into short xylooligosaccharides by a general acid–base mechanism involving two glutamic acid residues [1,2]. Typically, these enzymes can be classified into glycoside hydrolase (GH) families 10 and 11 based on amino-acid sequence similarities [3]. However, xylanases belonging to families 5, 8 and 43 have also been identified [4,5]. The biotechnological applications of xylanases include food, feed, textile and paper industries [6], and recently they have received much attention owing to their use in degradation of lignocellulosic biomass for biofuels production [7,8]. In this context, enzymes exhibiting high enzymatic efficiency combined with hyper thermal and chemical tolerance are extremely desired. Although countless extremophilic enzymes have been characterized, the molecular basis for their mode of action at high temperatures is still poorly understood. Several structures of family 10 xylanases have been solved, from mesophilic to hyperthermophilic organisms enabling an in-depth comparative study in terms of thermophilicity, thermostability and action mechanism. Thus, in order to gain insights into the structural determinants of their mode of action at high temperatures we have performed a functional and structural characterization of a hyperthermostable xylanase 10B from the bacterium *Thermotoga petrophila* RKU-1 (TpXyl10B). Our studies addressed important

Abbreviations: TpXyl10B, xylanase 10B from *Thermotoga petrophila* RKU-1; TmXyl10B, xylanase 10B from *Thermotoga maritima* MSB8; GH, glycoside hydrolase; CD, circular dichroism; CZE, capillary zone electrophoresis; U, unit; MD, molecular dynamics; XTAL, X-ray crystallography.

* Corresponding author. Address: Laboratório Nacional de Biociências (LNBio), Centro Nacional de Pesquisa em Energia e Materiais, Rua Giuseppe Maximo Scolfaro, 10000, Campinas, 13083-970 SP, Brazil. Fax: +55 19 3512 1004.
E-mail address: mario.murakami@lnbio.org.br (M.T. Murakami).

0006-291X © 2010 Elsevier Inc. Open access under the Elsevier OA license.
doi:10.1016/j.bbrc.2010.11.010

issues in the structure–function relationship of xylanases 10B as the modulation of their action mode at high temperatures by conformational changes in the product release area.

2. Material and methods

2.1. Cloning, protein expression and purification

The TpXyl10B coding gene was amplified by PCR using the *T. petrophila* RKU-1 genomic DNA as template and the following oligonucleotides: 5′-CATATGCAAAATGTATCTCTGAGAGAGCTC-3′ and 5-GGATCCTCATTCTATCTTTTTCTCCAGCAC-3′. The sequence was cloned into pGEM®-T Easy vector system (Promega) and was further subcloned into pET28a vector (Novagen) using *Nde*I and *Bam*HI restriction sites. The protein expression was performed in BL21(DE3)SlyD cells at 37 °C for 4 h after induction with 0.5 mM isopropyl β-D-1-thiogalactopyranoside. Harvested cells were resuspended in lysis buffer (20 mM sodium phosphate pH 7.4, 500 mM NaCl and 5 mM imidazole) and disrupted by lysozyme treatment (80 μg/mL, 1 h, on ice) followed by sonication (Vibracell VCX 500, Sonics & Materials, Inc.). The cell extract was clarified by centrifugation at 20,000*g* for 30 min at 4 °C and applied into a 5 mL HiTrap™ Chelating HP column (GE Healthcare) with a flow rate of 1 mL/min. The elution was carried out using an imidazole gradient from 5 to 500 mM in 20 column volumes. Fractions containing TpXyl10B were pooled, concentrated and applied into a Superdex 75 16/60 column (GE Healthcare) with a flow rate of 0.5 mL/min. All chromatographic steps were performed using an ÄKTA FPLC system (GE Healthcare). The purified TpXyl10B was then dialyzed against 20 mM phosphate buffer (pH 7.2) and concentrated by ultrafiltration. Sample purity was assessed by SDS–PAGE under reducing conditions. Protein concentration was determined by absorbance at 280 nm.

2.2. Xylanase activity assay

Xylanase activity was assayed using birchwood xylan (Sigma, USA) as substrate. Liberated reducing sugars were quantified by a dinitrosalicylic method [9]. One unit (U) of enzyme activity was defined as the amount of enzyme required to release 1 μmol of reducing sugar per minute. Specific activity was expressed as IU/mg protein.

2.3. Response surface methodology

The variables analyzed here were the pH along with temperature. Central points for 12 experiments in total were considered for optimization of these variables. Details regarding the statistical approaches for these experiments can be found in Myers and Montgomery [10]. The regression and graphical analysis of the data were performed using the software Statistica™ version 8.0, considering a *p*-value of 0.05. The significance of the regression coefficients was given by Student's *t*-test. The second order model equation was determined by Fisher's test and the multiple coefficient of determination (R^2) gave the variance explained by the model. All xylanase activity assays were carried out in triplicate using 10 μL of enzyme sample (650 ng), 40 μL of 50 mM acetate or phosphate buffer and 50 μL of birchwood xylan (stock solution 1%(W/V) in water).

2.4. Capillary zone electrophoresis of oligosaccharides

The 1,4-β-D-xylohexaose (Megazyme) was derivatized with 8-aminopyreno-1,3,6-trisulfonic acid (APTS) by reductive amination [11]. Capillary zone electrophoresis (CZE) of oligosaccharides was performed on a P/ACE MQD instrument (Beckman Coulter) equipped with laser-induced fluorescence detection. A fused-silica capillary (TSP050375, Polymicro Technologies) of internal diameter of 50 μm and total length of 31 cm was used as separation column for oligosaccharides. Electrophoresis conditions were 15 kV/70–100 μA at a controlled temperature of 20 °C. Oligomers labeled with APTS were excited at 488 nm and emission was collected through a 520 nm band pass filter.

2.5. Circular dichroism spectroscopy

Far-UV circular dichroism (CD) spectra were recorded on a Jasco J-810 spectropolarimeter (Jasco International Co.). CD measurements were carried out in a 1 mm quartz cuvette using the wavelength range of 190–260 nm. The protein concentration was set to 3.2 μM in 10 mM sodium phosphate buffer, pH 6.7. All samples were centrifuged at 10,000*g* for 10 min prior to analysis. In order to study the effect of temperature on TpXyl10B structure, the sample was heated from 20 to 95 °C and CD spectra at different temperatures were obtained. The data collection parameters were set to scan rate of 50 nm/min, response time of 4 s, sensitivity of 100 mdeg, accumulation of 6, heating rate of 1 °C/min and delay time for spectrum collection of 60 s. The reversibility of the temperature effect was checked by cooling the sample to 20 °C using the same parameters above. Baseline subtraction, smoothing and data normalization were carried out using the graphical software ORIGIN (http://www.originlab.com/). The CD data are shown as mean residue ellipticity units (deg cm^2 $dmol^{-1}$ $residue^{-1}$).

2.6. Crystal structure determination

Crystallization was performed by vapor diffusion method using a HoneyBee 963 robot (Genomic Solutions). Sitting drops were prepared by mixing 0.5 μL of Xyl10B at 8 mg/mL with an equal volume of mother liquor and were equilibrated against 80 μL of the solution at 18 °C. Small crystals grew from a solution containing 100 mM sodium acetate pH 4.5, 30%(W/V) PEG8000 and 200 mM lithium sulfate. The crystals were optimized by varying the pH or precipitant concentration in small steps. Best crystals grew in 5 days from the solution containing 100 mM sodium acetate pH 4.3, 14%(W/V) PEG8000, 200 mM lithium sulfate and 5%(V/V) glycerol. The TpXyl10B/xylobiose crystals were obtained by the co-crystallization method. The protein was incubated with 5 mM of both 1,4-β-D-xylohexaose (Megazyme) and xylose (Megazyme) and then used in crystallization experiments as previously described. Other substrates such as xylobiose, xylotriose, xylotetraose and xylopentaose were not tried for co-crystallization experiments. For X-ray data collection, crystals were taken from the drop and directly flash-cooled without adding any cryoprotectant in a 100 K nitrogen gas stream. X-ray diffraction data were collected at the W01B-MX2 beamline (Brazilian Synchrotron Light Laboratory, Campinas, Brazil). The wavelength used was 1.4586 Å and the intensities were recorded in a Mar Mosaic 225 mm CCD detector. A total of 360 images were collected with an oscillation angle of 1° for the native crystal and 175 images were collected with an oscillation of 2° for the TpXyl10B/xylobiose crystal. Data were indexed, integrated and scaled using the HKL2000 package [12]. The native structure of TpXyl10B was determined by molecular replacement method using the program MOLREP [13] and the atomic coordinates of TmXyl10B (PDB entry code: 1VBU, [14]) as the search model. The crystallographic structure was refined by interspersed cycles of manual model building based on inspection of the 2*Fo–Fc* and *Fo–Fc* maps using the program COOT [15] and restrained refinement with the program REFMAC5 [16]. Water molecules were manually added at the final stages.

Stereochemistry of the models was analyzed with the program PROCHECK [17].

2.7. Molecular dynamics simulations

The molecular dynamics (MD) simulations were performed with the TpXyl10B crystal structure using GROMACS suite and GROMOS96 43a1 force field [18]. The MD protocol was based on previous studies [19] evaluating the TpXyl10B structure at 20 °C (293 K) and 90 °C (363 K) for 20 ns. The systems were solvated in triclinic boxes using periodic boundary conditions and SPC water model [20]. Counter ions were added to neutralize the system. The Lincs method was applied to constrain covalent bond lengths, allowing an integration step of 2 fs after an initial energy minimization step using the steepest descents algorithm. Electrostatic interactions were calculated with Particle-Mesh Ewald [21]. Temperature and pressure were kept constant by separately coupling protein, ions, and solvent to external temperature and pressure baths [22] with coupling constants of $\tau = 0.1$ and 0.5 ps, respectively. The systems were slowly heated from 50 K to desired temperature (293 or 363 K) in steps of 5 ps, each one increasing the reference temperature by 50 K. The analyses were performed over the entire MD trajectories (details are given in Supplementary Fig. S1).

3. Results and discussion

3.1. Xylanase activity optimization

After the screening of variables by previous univariate experiments, a central composite design with two variables [23] and four center points was performed. The design matrix and the response results for xylanase activity are provided in supplementary Table S2. A model of two variable described by the equation IU/mg protein = $175.74 + 49.27X_1 - 57.72X_1^2 - 17.11X_2^2$ was used. The model was validated by variance analysis (ANOVA) indicating that the model was significant at high confidence level (95%), with $R^2 = 0.88$ [23,24]. The xylanase activity response was straight as expected, varying linearly with the pH and quadratically with the pH and temperature (Supplementary Fig. S3). The best conditions of enzyme activity were reached in the pH and temperature range of 6.2–7.0 and 79–90 °C, respectively. The best conditions obtained by the model (pH 6.5 and 88.2 °C) is in full agreement with those values obtained by univariate experiments (pH 6.5 and 90 °C) and the predicted xylanase activity (188.1 IU/mg protein) varied only 2% in respect to the experimental value (192.2 IU/mg protein) that is explained by the lack of fitness of the model in the periphery of the curve. The values found for TpXyl10B are similar to those shown for TmXyl10B, whose optimum pH and temperature are 6.1 and 90 °C, respectively [25]. In fact, these xylanases have great potential to be explored in industrial processes due to high thermostability and thermophilicity.

3.2. TpXyl10B produces exclusively xylobiose from xylohexaose at the optimum temperature

The product of enzymatic hydrolysis of xylohexaose by TpXyl10B at 20 or 90 °C were analyzed by CZE, indicating a temperature-dependent pattern of cleavage (Fig. 1A and B). Interestingly, at 20 °C both xylobiose and xylotriose were released by action of TpXyl10B (Fig. 1A), whereas at 90 °C only xylobiose was detected (Fig. 1B). The preference for xylobiose release was also reported for TmXyl10B [26], in an experiment carried out at 90 °C, similar to our results.

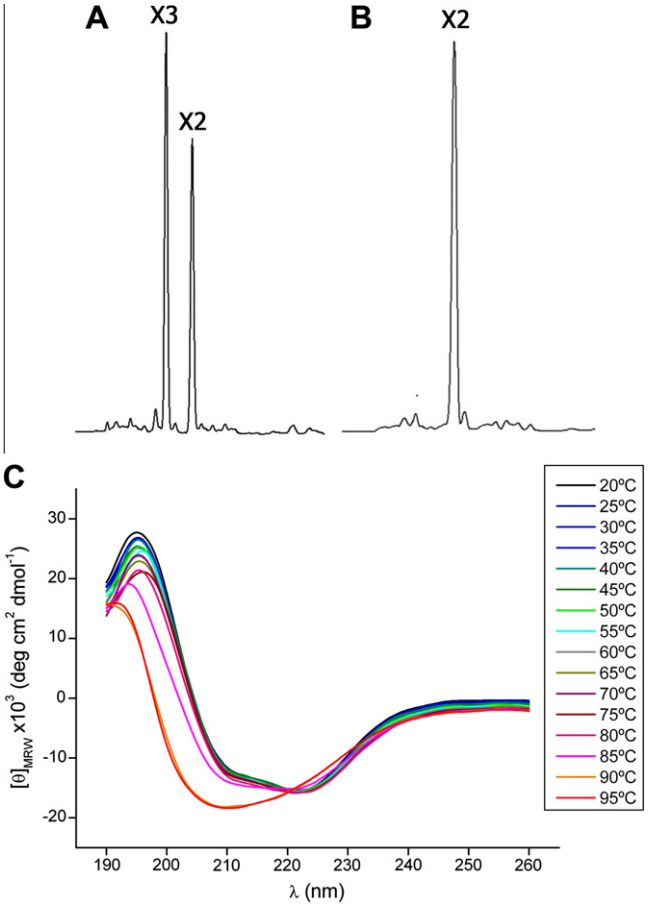

Fig. 1. Capillary zone electrophoresis of APTS-labeled oligosaccharides released through TpXyl10B enzymatic hydrolysis at 20 °C (A) or 90 °C (B). (C) Thermal stability of TpXyl10B as assessed by Far-UV CD experiments.

3.3. Secondary structure changes of TpXyl10B during heating

The Far-UV CD spectrum of Xyl10B at 20 °C showed a characteristic curve of α/β proteins with a maximum at 195 nm and a minimum at 222 nm (Fig. 1C). During heating from 20 to 95 °C, the CD spectrum presented significant alterations in its profile and amplitude at temperatures around 90 °C (Fig. 1C) indicating the occurrence of changes in the secondary structure contents of TpXyl10B. The optimum temperature for enzymatic activity is 90 °C suggesting that those structural changes would be associated with the TpXyl10B function. CD experiments were also performed in the presence of xylohexaose, which resulted in very similar CD spectral profiles like those obtained for the protein in the absence of substrate (results not shown).

3.4. Structure and substrate-binding sites

Co-crystallization of TpXyl10B with xylohexaose resulted in xylobiose bound at the active site, since xylohexaose has been hydrolyzed by the action of TpXyl10B. TpXyl10B was also co-crystallized in the presence of xylose; however, data analysis clearly indicated the presence of xylobiose bound to the active site instead of xylose. It could be explained by contamination of xylose with other xylan degradation products or due to a putative transglycosylation activity. Zhengqiang et al. [25] reported the formation of xylobiose after reaction of *p*-nitrophenyl-β-D-xylopyranoside by TmXyl10B and it was attributed to a transglycosylation reaction.

Table 1
Data collection and refinement statistics for TpXyl10B structures (Values in parentheses correspond to the last resolution shell).

	Native	Xylobiosecomplex
Data collection		
Space group	P1	P1
Unit cell parameters (Å, °)	a = 58.54, b = 58.55, c = 61.58, α = 84.54, β = 70.82, γ = 68.87	a = 58.34, b = 58.58, c = 61.66, α = 84.90, β = 70.86, γ = 68.93
Resolution (Å)	30.00–1.58 (1.64–1.58)	30.00–1.90 (1.97–1.90)
No. of observed reflections	348,387	196,749
No. of unique reflections	91,930 (8533)	53,633 (5257)
Completeness (%)	92.8 (86.8)	94.1 (92.2)
Rmerge[a]	10.1 (36.8)	11.2 (35.1)
I/σ(I)	11.2 (3.1)	11.6 (4.1)
Refinement		
Rfactor/Rfree(%)	15.79/19.55	23.06/29.85
Average B-factor (Å^2)	16.64	17.60
r.m.s.d. for bond lengths (Å)	0.021	0.023
r.m.s.d. for bond angles (°)	1.542	1.864
Ramachandran plot		
Most favored region (%)	90.8	88.7
Additional allowed (%)	9.2	11.3
Disallowed region (%)	0	0
PDB entry code	3NIY	3NJ3

[a] $R_{merge} = \Sigma_{hkl}\Sigma_i \mid I_i(hkl) - \langle I(hkl)\rangle \mid / \Sigma_{hkl}\Sigma_i I_i(hkl)$, where $I_i(hkl)$ is the ith observation of reflection $hkl$and $\langle I(hkl)\rangle$ is the weighted average intensity for all observations i of reflection hkl.

Our finding may be an indicative of transglycosylation activity for TpXyl10B since both proteins share 98% of sequence identity.

The native and xylobiose-complex structures of TpXyl10B have been determined at 1.58 and 1.90 Å, respectively. Native and xylobiose-complex crystals of TpXyl10B belonged to the triclinic P1 space group with two molecules in the asymmetric unit. Both structures present good overall stereochemistry (Table 1) with small r.m.s. deviations between native and complex structures suggesting that the presence of xylobiose did not result in significant alterations of protein conformation and consequently the crystal packing contacts.

TpXyl10B presents a classical $(\beta/\alpha)_8$ barrel (TIM barrel) fold conserving all the structural features described for TmXyl10B structure (Fig. 2A). The active site is located at the groove formed by the $\beta-\alpha$ elements-connecting loops at the interfacial face, which encompasses the two catalytic glutamic acid residues (Glu150 and Glu256). As observed for other Xyl10B structures, the cysteine residues at the positions 278 and 328 are 4.55 Å away from each other indicating a reduced state. If the Cys328 residue adopts a different rotameric conformation, the distance would be 2.26 Å and the disulfide bond could be formed.

In the xylobiose/TpXyl10B complex, the xylose1 residue at the −1 subsite makes hydrogen bonds with both catalytic residues and additionally with Lys68, His101, Asn149 and Gln225 side chains (Fig. 2B). The xylose1 also has van der Waals interactions with Trp305 as observed in the TmXyl10B structure. The xylose2 at the −2 subsite makes hydrogen bonds with Asn65, Glu64, Gln108, Lys68 and Trp297 side chains (Fig. 2B).

The highly similar TmXyl10B has also been crystallized in complex with xylobiose (PDB entry code: 1VBR) [14]. Despite the

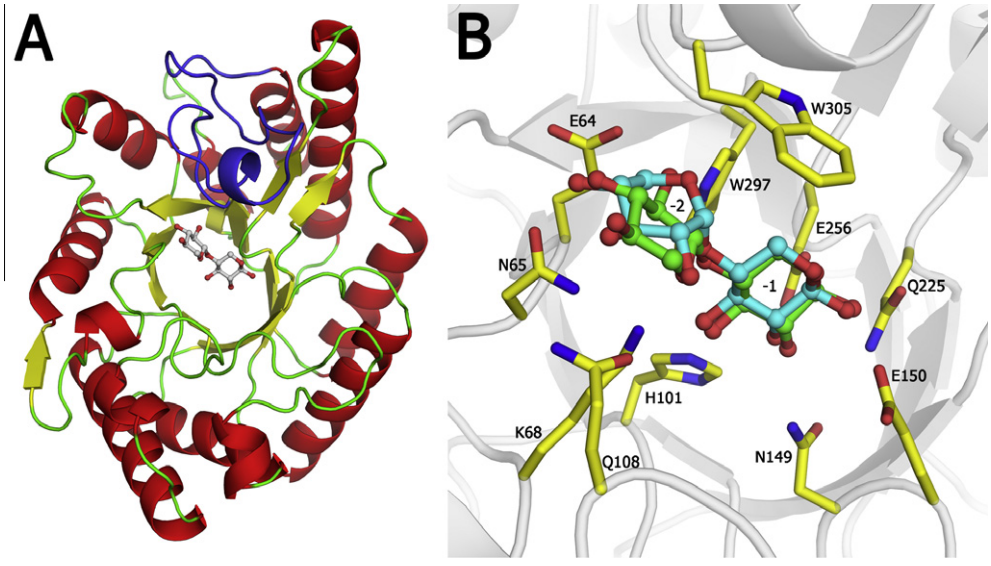

Fig. 2. Structure of TpXyl10B in complex with xylobiose. (A) Cartoon representation of the overall structure showing the ligand bound to the $(\beta/\alpha)_8$ barrel structure. (B) Superposition of the xylobiose from TmXyl10B (cyan; PDB code: 1VBU) structure on the TpXyl10B structure highlighting the differences on the mode of binding. The carbon atoms from TpXyl10B residues and the corresponding xylobiose are colored in yellow and green, respectively. All other atoms are shown in standard colors. (For interpretation of the references to colour in this figure legend, the reader is referred to the web version of this article.)

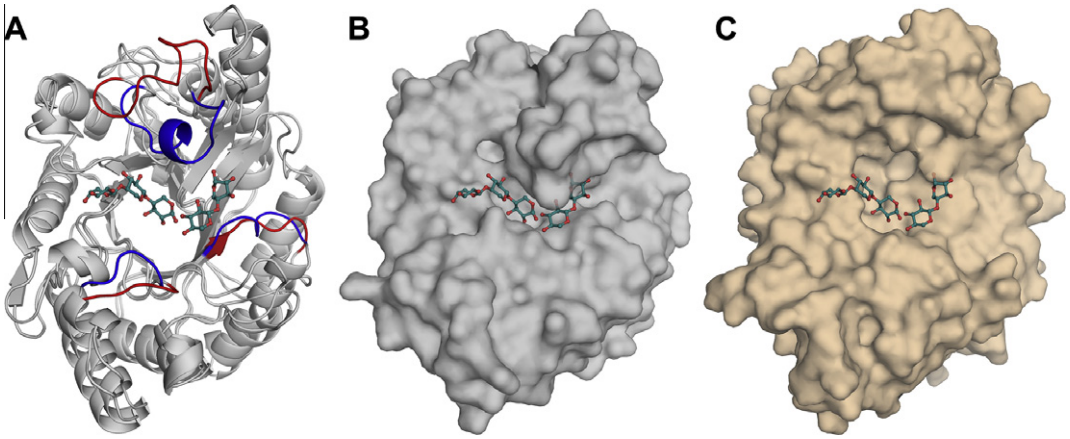

Fig. 3. Structural changes in the interfacial loops at 90 °C modulate enzymatic specificity of TpXyl10B. (A) The structure of TpXyl10B from molecular dynamics simulations at 90 °C was superposed on the native crystal structure and the main differences are colored in blue (crystal) and red (simulation). Molecular surface representations of the crystal structure (B) and the final frame from MD simulation at 90 °C (C). The *P. simplicissimum* xylopentaose complex structure (PDB entry code: 1B3Z) was superposed on the TpXyl10B structure and the xylopentaose is shown in the TpXyl10B active site to delineate the −3 to +2 subsites. (For interpretation of the references to colour in this figure legend, the reader is referred to the web version of this article.)

strong conservation of sequence between TpXyl10B and TmXyl10B (five divergent residues, located at the protein surface), the xylobiose at the active site is in a different conformation for these two xylanases (Fig. 2B). The xylose2 from TpXyl10B is rotated about 180° with respect to the corresponding xylose in the TmXyl10B structure. In other xylanases structures with longer substrates like xylotriose (PDB entry code: 2W5F; [27]) and xylotetraose (PDB entry code: 1US2; [28]), the xylose subunit at the −2 subsite displays a classical conformation as observed in our xylobiose-TpXyl10B complex structure. Interestingly, the active-site residues contacting xylobiose are exactly in the same position when compared to the xylobiose-TmXyl10B structure indicating that the unusual conformation observed in the TmXyl10B structure may be due to a misinterpretation of electron density map.

3.5. Structural basis for the mode of action at the optimum temperature

The enzymatic hydrolysis of xylan by endo-xylanases occurs between xylose residues at the −1 and +1 subsites. The xylose numbering follows sugar binding site nomenclature for glycosyl hydrolases [29]. These sites are well known, as shown for xylanases 10B from *Clostridium thermocellum*, *Cellvibrio japonicus* and *Penicillium simplicissimum* [27,28,30]. The −1, −2, −3 subsites were called "substrate recognition area" and +1,+2,+3 subsites were called "product release area" by Schmidt [30]. The substrate recognition area contains residues making abundant interactions with the ligand, whereas the product release area residues present fewer interactions with the ligand. It has been proposed that the negative subsites determine the minimum length of the substrate for catalysis indicating that xylotetraose is the shortest hydrolyzable substrate for xylanases 10B [30]. Herein, we propose a key role of the positive subsites in determining the product cleavage pattern of xylanases 10B.

As observed by CZE analysis, TpXyl10B releases exclusively xylobiose at temperatures close to 90 °C (Fig. 1B) and it is correlated with significant structural changes under the same conditions as assessed by CD spectroscopy (Fig. 1C). In order to shed light on the molecular basis of the temperature influence on the action mode of TpXyl10B, molecular dynamics simulations were carried out at 20 and 90 °C.

The final frame of TpXyl10B structure from MD simulations at 90 °C presented only significant differences around the product release area when compared to the crystal structure, without disturbing the overall fold and structure (Fig. 3). At 90 °C, the catalytic loop comprising the residues 297–326 was displaced far away from its original conformation, resulting in a drastic increase of accessible solvent area (ASA) of the active-site pocket and in the loss of the +3 subsite. Contrary to the fact that the increase of ASA around to the active site could accommodate larger substrates, the loss of the +3 subsite does not permit the binding of additional xylose subunits at the product release area. Additionally, the displacement of the catalytic loop has also disturbed the adjacent +2 subsite contributing to specific release of xylobiose at the optimum temperature.

In conclusion, our findings from CD, CZE, XTAL and MD studies suggest that thermal-induced conformational changes in the product release area play a role in the modulation of the action mode of thermostable xylanases 10B.

Acknowledgments

This research was supported by grants from Fundação de Amparo à Pesquisa do Estado de São Paulo (FAPESP, 08/58037-9) to FMS and Conselho Nacional de Desenvolvimento Científico e Tecnológico (CNPq, 478059/2009-4 and 472174/2007-0) to MTM and HV, respectively. RAP has funding from the Department of Energy, awards 06103-OKL and ZDJ-7-77608-01.

Appendix A. Supplementary data

Supplementary data associated with this article can be found, in the online version, at doi:10.1016/j.bbrc.2010.11.010.

References

[1] J.D. McCarter, S.G. Withers, Mechanisms of enzymatic glycoside hydrolysis, Curr. Opin. Struct. Biol. 4 (1994) 885–892.
[2] G. Davies, B. Henrissat, Structures and mechanisms of glycosyl hydrolases, Structure 3 (1995) 853–859.
[3] B. Henrissat, G. Davies, Structural and sequence-based classification of glycoside hydrolases, Curr. Opin. Struct. Biol. 7 (1997) 637–644.
[4] B. Henrissat, A. Bairoch, New families in the classification of glycosyl hydrolases based on amino acid sequence similarities, Biochem. J. 293 (1993) 781–788.
[5] B.L. Cantarel, P.M. Coutinho, C. Rancurel, T. Bernard, V. Lombard, B. Henrissat, The carbohydrate-active enzymes database (CAZy): an expert resource for glycogenomics, Nucleic Acids Res. 37 (2009) D233–D238.
[6] N. Kulkarni, A. Shendye, M. Rao, Molecular and biotechnological aspects of xylanases, FEMS Microbiol. Rev. 23 (1999) 411–456.

[7] J. Sheehan, M. Himmel, Enzymes, energy, and the environment: a strategic perspective on the U.S. Department of energy's research and development activities for bioethanol, Biotechnol. Prog. 15 (1999) 817–827.
[8] J. Zaldivar, J. Nielsen, L. Olsson, Fuel ethanol production from lignocellulose: a challenge for metabolic engineering and process integration, Appl. Microbiol. Biotechnol. 56 (2001) 17–34.
[9] G. Miller, Use of dinitrosalicylic acid reagent for determination of reducing sugar, Anal. Chem. 31 (1959) 426–428.
[10] R.H. Myers, D.C. Montgomery, Response surface methodology: process and product optimization using designed experiments, John Wiley & Sons, New York, 2002, pp. 1–13.
[11] F.T. Chen, R.A. Evangelista, Analysis of mono- and oligosaccharide isomers derivatized with 9-aminopyrene-1, 4, 6-trisulfonate by capillary electrophoresis with laser-induced fluorescence, Anal. Biochem. 230 (1995) 273–280.
[12] Z. Otwinowski, W. Minor, Processing of X-ray diffraction data collected in oscillation mode, Methods Enzymol. 276 (1997) 307–326.
[13] A. Vagin, A. Teplyakov, MOLREP: an automated program for molecular replacement, J. Appl. Crystallogr. 30 (1997) 1022–1025.
[14] Ihsanawati, T. Kumasaka, T. Kaneko, C. Morokuma, R. Yatsunami, T. Sato, S. Nakamura, N. Tanaka, Structural basis of the substrate subsite and the highly thermal stability of xylanase 10B from *Thermotoga maritima* MSB8, Proteins 61 (2005) 999–1009.
[15] P. Emsley, K. Cowtan, Coot: model-building tools for molecular graphics, Acta Crystallogr. D 60 (2004) 2126–2132.
[16] G.N. Murshudov, A.A. Vagin, E.J. Dodson, Refinement of macromolecular structures by the maximum-likelihood method, Acta Crystallogr. D 53 (1997) 240–255.
[17] R.A. Laskowski, M.W. MacArthur, D.S. Moss, J.M. Thornton, PROCHECK - a program to check the stereochemical quality of protein structures, J. Appl. Crystallogr. 26 (1993) 283–291.
[18] D. van der Spoel, E. Lindahl, B. Hess, G. Groenhof, A.E. Mark, H.J.C. Berendsen, GROMACS: fast, flexible and free, J. Comput. Chem. 26 (2005) 1701–1718.
[19] B.L. de Groot, H. Grubmüller, Water permeation across biological membranes: mechanism and dynamics of aquaporin-1 and GlpF, Science 294 (2001) 2353–2357.
[20] H.J.C. Berendsen, J.P.M. Postma, W. van Gunsteren, J. Hermans, Interaction models for water in relation to protein hydration, in: B. Pullman (Ed.), Intermolecular Forces, Dordrecht Reidel Publishing Company, The Netherlands, 1981, pp. 331–342.
[21] T. Darden, D. York, L. Pedersen, Particle mesh Ewald – an N log(N) method for Ewald sums in large systems, J. Chem. Phys. 98 (1993) 10089–10092.
[22] H.J.C. Berendsen, J.P.M. Postma, A. DiNola, J.R. Haak, Molecular dynamics with coupling to an external bath, J. Chem. Phys. 81 (1984) 3684–3690.
[23] F. Francis, A. Sabu, K.M. Nampoothiri, S. Ramachandram, S. Ghosh, G. Szakacs, A. Pandey, Use of response surface methodology for optimizing process parameters for the production of α-amylase by *Aspergillus oryzae*, Biochem. Eng. J. 15 (2003) 107–115.
[24] F.F.C. Barros, J.L. Bicas, J.C. Silva, A.P. Dionisio, G.M. Pastore, Use of the response surface methodology to optimize the pre-treatment of cassava wastewater employed as substrates for the production biosurfactants, in: J. Krause, O. Fleischer (Eds.), Industrial Fermentation: Food Processes, Nutrient Sources and Production Strategies, Nova Science Publisher, Hauppauge, New York, 2010, pp. 327–341.
[25] J. Zhengqiang, A. Kobayashi, M.M. Ahsan, L. Lite, M. Kitaoka, K. Hayashi, Characterization of a thermostable family 10 endo-xylanase (XynB) from *Thermotoga maritima* that cleaves *p*-nitrophenyl-beta-D-xyloside, J. Biosci. Bioeng. 92 (2001) 423–428.
[26] Z.Q. Jiang, W. Deng, Y.P. Zhu, L.T. Li, Y.J. Sheng, K. Hayashi, The recombinant xylanase B of *Thermotoga maritima* is highly xylan specific and produces exclusively xylobiose from xylans, a unique character for industrial applications, J. Mol. Catal. B Enzym. 27 (2004) 207–213.
[27] S. Najmudin, B.A. Pinheiro, J.A. Prates, H.J. Gilbert, M.J. Romão, C.M. Fontes, Putting an N-terminal end to the *Clostridium thermocellum* xylanase Xyn10B story: crystal structure of the CBM22–1-GH10 modules complexed with xylohexaose, J. Struct. Biol. 172 (2010) 353–362.
[28] G. Pell, L. Szabo, S.J. Charnock, H. Xie, T.M. Gloster, G.J. Davies, H.J. Gilbert, Structural and biochemical analysis of *Cellvibrio japonicus* xylanase 10C: how variation in substrate-binding cleft influences the catalytic profile of family GH-10 xylanases, J. Biol. Chem. 279 (2004) 11777–11788.
[29] G.J. Davies, K.S. Wilson, B. Henrissat, Nomenclature for sugar-binding subsites in glycosyl hydrolases, Biochem. J. 321 (1997) 557–559.
[30] A. Schmidt, G.M. Gübitz, C. Kratky, Xylan binding subsite mapping in the xylanase from *Penicillium simplicissimum* using xylooligosaccharides as cryoprotectant, Biochemistry 38 (1999) 2403–2412.